

Original paper

Nickel- and Fe³⁺-rich oxy-dravite from the Artana Mn prospect, Apuan Alps (Tuscany, Italy)

Daniela MAURO¹, Cristian BIAGIONI^{2*}, Ulf HÅLENIUS³, Henrik SKOGBY³, Valentina DOTTORINI², Ferdinando BOSI⁴

¹ Museo di Storia Naturale, Università di Pisa, Via Roma 79, I-56011 Calci (PI), Italy

² Dipartimento di Scienze della Terra, Università di Pisa, Via Santa Maria 53, I-56126 Pisa, Italy; cristian.biagioni@unipi.it

³ Department of Geosciences, Swedish Museum of Natural History, P.O. Box 50 007, SE-10405 Stockholm, Sweden

⁴ Dipartimento di Scienze della Terra, Sapienza Università di Roma, Piazzale Aldo Moro 5, I-00185 Rome, Italy

* Corresponding author



Nickel- and Fe³⁺-rich oxy-dravite was identified on a specimen collected in the Artana Mn prospect, Carrara, Apuan Alps, Tuscany, Italy. Oxy-dravite occurs as brownish-orange prismatic crystals, up to 0.3 mm in length, associated with quartz, carbonates, and hematite. Electron microprobe analysis gave (in wt. % – average of 7 spot analyses): SiO₂ 35.81, TiO₂ 0.41, B₂O_{3(cal)} 10.38, Al₂O₃ 29.36, V₂O₃ 0.78, Cr₂O₃ 0.09, Fe₂O₃ 3.32, FeO 0.33, MgO 8.04, CaO 0.39, MnO 0.34, NiO 3.46, ZnO 0.40, Na₂O 2.84, F 0.29, H₂O_(cal) 3.00, O = F – 0.12, total 99.12. The Fe³⁺/Fe_{tot} ratio was calculated based on optical absorption spectroscopy. The empirical ordered formula of the studied sample is (with rounding errors) ^X(Na_{0.92}Ca_{0.07□})_{Σ1.00}^Y(Mg_{2.01}Ni_{0.47}Fe³⁺_{0.33}Ti_{0.05}Mn²⁺_{0.05}Fe²⁺_{0.05}Zn_{0.05})_{Σ3.00}^Z(Al_{5.80}V_{0.10}Cr_{0.01}Fe³⁺_{0.09})_{Σ6.00}Si₆O₁₈(BO₃)₃^V(OH)₃^W[O_{0.50}(OH)_{0.35}F_{0.15}]_{Σ1.00}. This is an intermediate member of the dravite–oxy-dravite series. In naming it, the prefix oxy- was preferred since ^WO is very close to being larger than 0.5 atoms per formula unit. Infrared spectroscopy revealed the occurrence of significant amounts of ^W(OH), and allowed to propose a specific short-range arrangements around the O(1) and O(3) sites. Unit-cell parameters are *a* = 15.9349(11), *c* = 7.2038(5) Å, *V* = 1584.1(2) Å³, space group *R*3*m*. The crystal structure was refined by single-crystal X-ray diffraction data to *R*₁ = 0.0146 on the basis of 1138 unique reflections with *F*_o > 4σ(*F*_o) and 94 refined parameters. The optimized crystal-chemical formula is ^X(Na_{0.92}Ca_{0.07□})_{Σ1.00}^Y(Mg_{1.21}Al_{0.80}Ni²⁺_{0.47}Fe³⁺_{0.26}Ti_{0.05}Mn²⁺_{0.05}Zn_{0.05}V_{0.10}Cr_{0.01})_{Σ3.00}^Z(Al_{5.00}Mg_{0.80}Fe³⁺_{0.16}Fe²⁺_{0.05})_{Σ6.00}Si₆O₁₈(BO₃)₃^{O(3)}(OH)₃^{O(1)}[O_{0.50}(OH)_{0.35}F_{0.15}]_{Σ1.00}. Nickel is ordered at the *Y* site, in agreement with results obtained on synthetic tourmalines. Oxy-dravite is likely the result of the metamorphic recrystallization of Mn-rich layers at the top of the Liassic carbonates belonging to the Marble Formation of the Apuan Alps Metamorphic Complex.

Keywords: tourmaline supergroup; oxy-dravite; nickel; crystal structure; Apuan Alps; Italy

Received: 29 November 2021; **accepted:** 10 June 2022; **handling editor:** J. Cempirek

The online version of this article (doi: 10.3190/jgeosci.346) contains supplementary electronic material.

1. Introduction

Tourmaline-supergroup minerals from Tuscany (Italy) are well known worldwide. Indeed, this Italian region is the type locality for seven species. Among them elbaite (Verdovsky 1913), tsilaisite (Bosi et al. 2012), fluor-tsilaisite (Bosi et al. 2015a), and celleriite (Bosi et al. 2022a) were found in vugs of granitic pegmatitic dykes in the San Piero in Campo area, Elba Island. This is a classic kind of occurrence that has been studied since the 19th century (e.g., D'achiardi 1894, 1897), providing nice specimens kept in several private and public collections worldwide.

Three additional species have been discovered during the crystal-chemical characterization of non-pegmatitic tourmalines from Tuscany. Uvite and magnesio-lucchiite were identified in veins within metabasite of the thermal aureole of the Monte Capanne intrusion (Bosi et al. 2022b; Scribner et al. 2021), whereas dutrowite was

discovered in a Permian metarhyolite belonging to the Apuane Metamorphic Complex (Biagioni et al. 2020).

Tourmaline supergroup minerals are common in rocks from the Apuan Alps and, in the southern sector of this area they form tourmalinite bodies closely associated with ore deposits (e.g., Benvenuti et al. 1989), in some cases spatially related to Permian metarhyolite (Vezzoni et al. 2018). Other minor occurrences have been reported from several localities (e.g., Orlandi and Dini 2004; Biagioni et al. 2019), but the only crystal-chemical data currently available were provided by Benvenuti et al. (1991) on tourmaline supergroup minerals occurring in tourmalinite associated with the Pb–Zn–Ag ore deposit formerly exploited at the Bottino mine.

During the examination of a suite of specimens from the small Artana Mn prospect on the northern slope of the mountain ridge La Rocchetta–Monte Brugiana, near Carrara (Apuan Alps, northern Tuscany), a sample con-

taining sub-millimetric prismatic crystals of a potential tourmaline supergroup mineral was identified. The mineralogical study confirmed the first identification, pointing out a high Ni content and suggesting the necessity of its full crystal-chemical investigation. Indeed, nickeloan tourmalines have been reported from a few localities worldwide (e.g., Henry and Dutrow 2001; Baksheev and Kudryavtseva 2004; Voudouris et al. 2019) and structural data have been mainly collected on synthetic analogs (e.g., Rozhdestvenskaya et al. 2012; Vereshchagin et al. 2015); the only natural refined sample was reported as triclinic (Hughes et al. 2011).

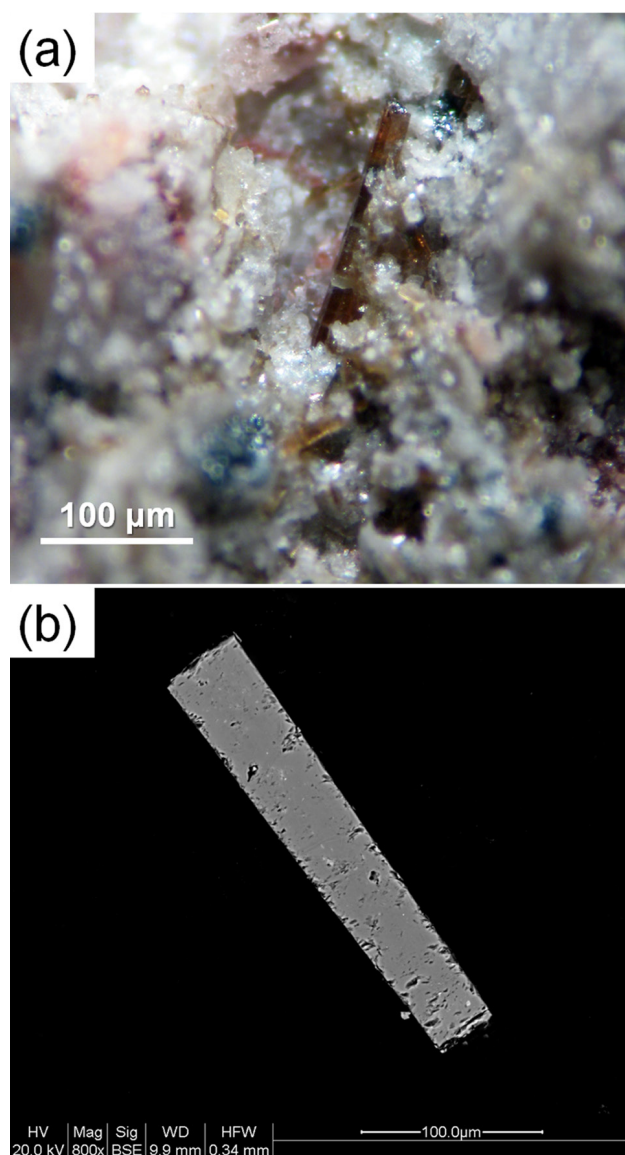


Fig. 1 Oxy-dravite from the Artana Mn prospect. (a) Brownish-orange crystals up to 0.2 mm, with carbonates. (b) Back-scattered electron image of the studied crystal. Collection of Natural History Museum of the University of Pisa, catalog number 19935.

In this paper, the crystal chemistry, genesis and geological implications of this new finding of a nickeloan tourmaline are reported.

2. Geological background and sample description

The Apuan Alps are a sector of the Northern Apennines where the lowermost tectonic units are exposed, i.e., the Massa Unit and the Apuane Unit. These units were affected by greenschist facies metamorphism during the late Oligocene to early Miocene, with peak estimates at $T = 350\text{--}450\text{ }^{\circ}\text{C}$ and $P = 0.3\text{--}0.4\text{ GPa}$ in the Apuane Unit (e.g., Franceschelli et al. 2004; Fellin et al. 2007). The current structural setting is due to two main tectono-metamorphic phases, i.e., a shortening D_1 event at 27 Ma followed by an extensional D_2 phase at 14–12 Ma (Kligfield et al. 1986; Carmignani and Kligfield 1990).

The Artana Mn mineralization occurs on the western and northern slopes of the Monte Zuccone, close to the Artana B marble quarry, and northern of the mountain ridge La Rocchetta–Monte Brugiana. According to Conti et al. (2019), the ore deposit, prospected in the first half of the 20th century, is located at the contact between cherty metalimestone and the Marble Formation belonging to the Apuane Unit. The Mn ore body has an average thickness of 50 cm, only locally being ca. 1 m thick. Its mineralogy (as well as its actual setting) is poorly known. Di Giovanni (1981) reported the occurrence of braunite, whereas Bonazzi et al. (1992) studied REE-bearing piemontite, also citing the presence of Mn-oxides, titanite, “apatite”, Al-Mg-Fe dioctahedral mica, some rhombohedral Mn-bearing Ca-carbonates, as well as spessartine, “allanite”, and actinolite. Finally, Orlandi (1990) reported the identification of gasparite-(Ce), associated with manganite, quartz, and hematite.

Some samples were collected in a short tunnel of the Artana Mn prospect in December 2011. Tourmaline occurs as brownish-orange prismatic crystals, up to 0.3 mm in length (Fig. 1a), associated with quartz, carbonates, and tabular crystals of hematite. The studied material is kept in the mineralogical collection of the Natural History Museum of the University of Pisa under catalog number 19935.

3. Methods and results

3.1. X-ray crystallography

Single-crystal X-ray diffraction intensity data were collected using a Bruker Apex II diffractometer (50 kV, 30 mA) equipped with a Photon II CCD detector and

graphite-monochromatized MoK_α radiation (Dipartimento di Scienze della Terra, Università di Pisa, Italy). The detector-to-crystal distance was set at 50 mm. A total of 1054 frames were collected using φ and ω scan modes in 0.5° slices, with an exposure time of 10 s per frame, and they were corrected for Lorentz, polarization, absorption and background effects using the software package Apex3 (Bruker AXS Inc. 2016). The refined unit-cell parameters are $a = 15.9349(11)$, $c = 7.2038 \text{ \AA}$, $V = 1584.1(2) \text{ \AA}^3$; space group $R3m$. The crystal structure of the studied sample was refined using SHELXL-2018 (Sheldrick 2015), starting from the structural model of oxy-vanadium-dravite (Bosi et al. 2013). The following neutral scattering curves, taken from the International Tables for Crystallography (Wilson 1992), were used: Na vs. Ca at the X site, Mg vs. Fe at the Y site, Al vs. Fe at the Z site. The T , B , and anion sites were modeled with Si, B and O scattering factors and with a fixed occupancy of 1, because refinement with unconstrained occupancies showed no significant deviations from this value. The anisotropic structural model for all atoms converged to $R_1 = 0.0146$ for 1138 unique reflections with $F_o > 4\sigma(F_o)$ and 94 refined parameters. Tab. 1 gives details of data collection and refinement, whereas fractional atomic coordinates, displacement parameters, and selected bond distances are given in the Crystallographic Information File (CIF), available as Electronic Supplementary Material.

Tab. 1 Summary of crystal data and parameters describing data collection and refinement for (Ni,Fe³⁺)-rich oxy-dravite.

Crystal data	
Crystal size (mm)	0.240 × 0.050 × 0.050
Space group	$R3m$
a (Å)	15.9349(11)
c (Å)	7.2038(5)
V (Å ³)	1584.1(2)
Z	3
Data collection and refinement	
Radiation, wavelength (Å)	MoK _α , $\lambda = 0.71073$
Temperature (K)	293(2)
$2\theta_{\text{max}}$ (°)	63.00
Measured reflections	8233
Unique reflections	1142
Reflections with $F_o > 4\sigma(F_o)$	1138
R_{int}	0.0216
$R\sigma$	0.0175
	$-23 \leq h \leq 21$,
	$-23 \leq k \leq 19$,
	$-10 \leq l \leq 10$
Range of h, k, l	
$R_1 [F_o > 4\sigma(F_o)]$	0.0146
R_1 (all data)	0.0146
wR_2 (on F_o^2)	0.0375
Goof	1.117
Number of least-squares parameters	94
Maximum and minimum residual peak ($e \text{ \AA}^{-3}$)	+0.28 [at 0.71 Å from X] −0.26 [at 0.30 Å from T]

3.2. Electron microprobe analysis

The crystal used for single-crystal X-ray diffraction was then embedded in epoxy and polished for chemical analysis. Back-scattered electron images and preliminary chemical data were collected using an FEI Quanta 450 ESEM FEG equipped with a Bruker QUANTAX XFlash detector 6|10 operating in EDS mode (C. I. S. U. P., University of Pisa, Italy). Back-scattered electron images showed the studied sample to be homogeneous (Fig. 1b).

Quantitative chemical analyses were carried out using a Cameca SX50 (Istituto di Geologia Ambientale e Geoingegneria, CNR, Rome, Italy). Experimental conditions were: accelerating voltage 15 kV, beam current 15 nA, beam diameter 10 μm . The following standards were used (element; K α lines were used for all elements): wollastonite (Si, Ca), rutile (Ti), corundum (Al), Cr₂O₃ (Cr), V₂O₃ (V), magnetite (Fe), metallic Mn (Mn), periclase (Mg), metallic Ni (Ni), sphalerite (Zn), jadeite (Na), and fluorophlogopite (F). The “PAP” routine was applied (Pouchou and Pichoir 1985). Results (average of 7 spot analyses) are given in Tab. 2. Due to the small amount of available material, the Fe³⁺/Fe_{tot} ratio cannot be directly determined, for instance, through Mössbauer spectroscopy. Therefore, this ratio was estimated based on polarized optical absorption spectroscopy (see below).

3.3. Single-crystal infrared spectroscopy

Polarized Fourier-transform infrared (FTIR) absorption spectra of the studied sample were recorded using a Bruker

Tab. 2 Chemical data for (Ni,Fe³⁺)-rich oxy-dravite.

Oxide	wt. %	Range	e.s.d.
SiO ₂	35.81	35.41–35.94	0.19
TiO ₂	0.41	0.30–0.62	0.14
B ₂ O ₃ (calc)	10.38		
Al ₂ O ₃	29.36	28.87–29.72	0.31
V ₂ O ₃	0.78	0.53–1.08	0.18
Cr ₂ O ₃	0.09	0.06–0.11	0.02
MgO	8.04	7.90–8.23	0.13
CaO	0.39	0.25–0.59	0.14
MnO	0.34	0.25–0.64	0.14
FeO _(tot)	3.32	2.65–3.94	0.40
NiO	3.46	3.00–4.09	0.43
ZnO	0.40	0.35–0.47	0.04
Na ₂ O	2.84	2.77–2.92	0.05
F	0.29	0.16–0.45	0.10
H ₂ O _(calc)	3.00		
O = F	−0.12		
^a Fe ₂ O ₃	3.32		
^a FeO	0.33		
Total	99.12		

^a from OAS data

e.s.d. = estimated standard deviation

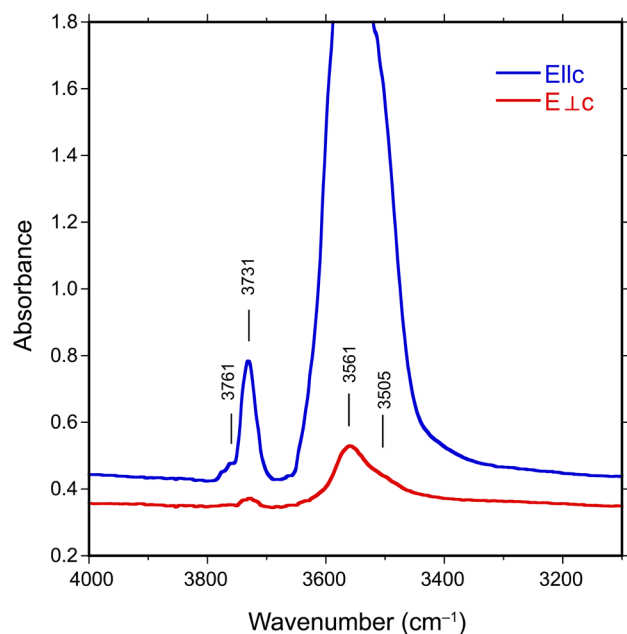


Fig. 2 Polarized Infrared spectra of (Ni,Fe³⁺)-rich oxy-dravite, vertically offset for clarity. The main band is truncated in the $E||c$ direction due to excessive absorption. Sample thickness 41 μm .

Vertex 70 microscope spectrometer (Swedish Museum of Natural History, Stockholm, Sweden) attached to a Hyperion 2000 microscope, using a halogen lamp source, a CaF₂ beam-splitter, a ZnSe polarizer, and an InSb detector. A crystal of lateral size of 60 × 200 μm was embedded in thermoplastic resin on a glass plate and polished to a thickness of 41 μm . Spectra were acquired from the central parts of the crystal over the wavenumber range 2000–13000 cm^{-1} during 500 cycles with a resolution of 4 cm^{-1} .

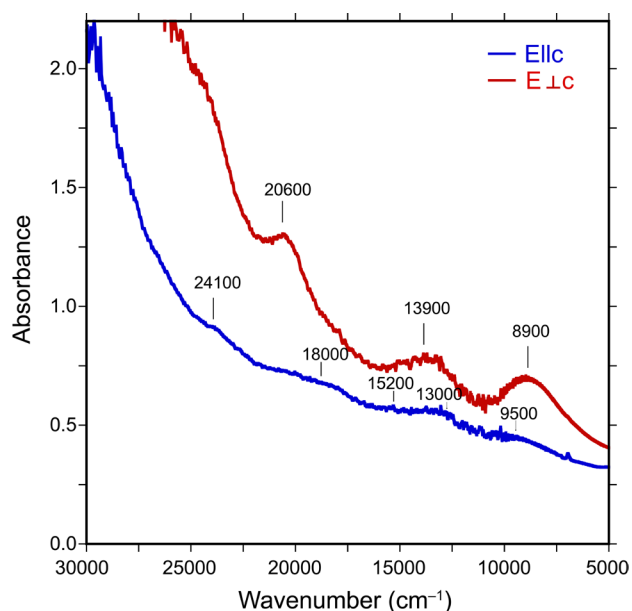


Fig. 3 Polarized optical absorption spectra of (Ni,Fe³⁺)-rich oxy-dravite. Sample thickness 41 μm .

The spectra recorded in polarized mode parallel to the c -axis ($E||c$) show a very intense band centered around 3550 cm^{-1} , which is off-scale as normally observed for tourmaline spectra, a significant band at 3731 cm^{-1} , and a weak band at 3761 cm^{-1} (Fig. 2). Spectra polarized perpendicular to the c -axis ($E\perp c$) show considerably weaker bands at 3561 and 3731 cm^{-1} , and a shoulder feature at 3505 cm^{-1} , as determined by spectral fitting. The occurrence of bands above 3650 cm^{-1} is consistent with a significant amount of (OH) groups at the O(1) site (see below). In detail, it is worth noting that the intensity of these bands, corresponding to ^w(OH)_{0.35} (see below), is slightly stronger than, but fully compatible with, the intensity of bands observed for vanadio-oxy-dravite with ^w(OH)_{0.26} (Bosi et al. 2014).

3.4. Optical Absorption Spectroscopy (OAS)

Polarized, room temperature optical absorption spectra in the range 30000–10000 cm^{-1} (333–1000 nm) were recorded at a spectral resolution of 1 nm on the same 41 μm thick section studied by FTIR spectroscopy, using an AVASPEC-ULS2048 × 16 spectrometer (Swedish Museum of Natural History, Stockholm, Sweden) attached via a 400 μm UV fiber cable to a Zeiss Axiotron UV-microscope. A 75 W Xe arc lamp was used as a light source, and Zeiss Ultrafluor 10 × lenses served as an objective and condenser. The size of the circular measure aperture was 30 μm across. A UV-quality Glan-Thompson prism with an operating range from 40000 to 3704 cm^{-1} (250 to 2700 nm) was used as a polarizer. The wavelength scale of the spectrometer was calibrated against Ho₂O₃-doped and Pr₂O₃/Nd₂O₃-doped standards (Hellma glass filters 666F1 and 666F7). Spectral data in the range 10000–2000 cm^{-1} (1000–5000 nm) was taken from the FTIR measurements.

The recorded $E\perp c$ ($E||O$) spectrum (Fig. 3) shows medium strong absorption bands at 20600, 13900, and 8900 cm^{-1} . In the $E||c$ ($E||E$) spectrum (Fig. 3) only weak to very weak bands occur at 24100, 20600, 18000, 15200, 13900, 13000, 9500, and 8900 cm^{-1} . The relatively sharp bands at 20600 and 18000 cm^{-1} are due to electronic transitions in Fe³⁺ pairs at neighboring Y -sites (Mattson and Rossman 1984). The relatively broad and distinctly $E\perp c$ -polarized bands at 13900 and 8900 cm^{-1} are assigned in agreement with previous optical studies of tourmaline (e.g., Mattson and Rossman 1987) to Fe³⁺-enhanced spin-allowed $d-d$ transitions in six-coordinated Fe²⁺. The very weak absorption bands at 24100, 15200, 13000, and 9500 cm^{-1} occur at energies close to those recorded for spin-allowed $d-d$ transitions in octahedrally coordinated Ni²⁺ in tourmaline (Taran et al. 1993). Based on the linear absorption coefficients reported for these absorption bands (Taran et al. 1993), combined with the Ni²⁺-content and absorber thickness of the present tourmaline, absorbance

values of merely 0.03 are expected for these bands, which compares well with what is observed. Additional sharp absorption bands that were observed in the $E||c$ -spectrum in the range 6700–7000 cm⁻¹ are attributed to overtones of the fundamental (OH)-stretching modes.

The relatively high intensity of the Fe³⁺ pair band at 20600 cm⁻¹ in combination with moderate intensities of the bands at 13900 and 8900 cm⁻¹ that are caused by Fe³⁺-enhanced spin-allowed $d-d$ transitions in six-coordinated Fe²⁺ strongly suggest that ferric iron dominates over ferrous in the present sample. A low fraction of ferrous iron is also underlined by the absence of a Fe²⁺–Ti⁴⁺ charge transfer band at 22000 cm⁻¹ (e.g., Taran et al. 1993) in the present optical absorption spectra, although the sample contains 0.41 wt. % TiO₂. Based on the molar absorption coefficient for the Fe³⁺ pair band at 20600 cm⁻¹ suggested by Mattson and Rossman (1984), the ferric iron content of the present tourmaline is calculated at 3.3 wt. % Fe₂O₃. With a total iron content of 3.69 wt. % Fe₂O₃, as determined by electron microprobe analyses, the resulting Fe³⁺/Fe_{tot} ratio becomes ~0.9, suggesting that the present tourmaline is indeed strongly oxidized. This is in keeping with the occurrence of hematite in close association with the studied tourmaline.

The brownish-orange color of the present tourmaline is determined mainly by a steep UV-absorption edge, which is caused mainly by the ligand to Fe³⁺ charge transfer processes, and by the relatively strong Fe³⁺ pair band absorption at 20600 cm⁻¹.

3.5. Determination of the number of atoms per formula unit (apfu)

In agreement with the structure-refinement results, the boron content was assumed to be stoichiometric (B³⁺ = 3.00 apfu). Both the site-scattering results and the bond lengths of *B* and *T* sites are consistent with the *B* site fully occupied by boron and no amount of B³⁺ at the *T* site (e.g., Bosi and Lucchesi 2007). The iron oxidation state was determined by OAS with Fe³⁺/Fe_{tot} = 0.9. In accordance with the OAS result and Fe and Mn redox potential arguments, all Mn was considered as Mn²⁺. Following Pesquera et al. (2016), the Li₂O content was assumed to be insignificant as MgO > 2 wt. % is contained in the sample studied. The (OH) content and the formula were

then calculated by charge balance with the assumption (T + Y + Z) = 15 apfu and 31 anions. The excellent agreement between the number of electrons per formula unit (epfu) derived from electron microprobe analysis and structure refinement (241.6 and 241.1 epfu, respectively) supports the stoichiometric assumptions.

4. Discussion

4.1. Crystal-chemistry of (Ni,Fe³⁺)-rich oxy-dravite

Following Henry et al. (2011), the empirical ordered formula of the studied sample is (with rounding errors) $^X(\text{Na}_{0.92}\text{Ca}_{0.07}\square_{0.01})_{\Sigma 1.00}^Y(\text{Mg}_{2.01}\text{Ni}_{0.47}\text{Fe}^{3+}_{0.33}\text{Ti}_{0.05}\text{Mn}^{2+}_{0.05}\text{Fe}^{2+}_{0.05}\text{Zn}_{0.05})_{\Sigma 3.00}^Z(\text{Al}_{5.80}\text{V}_{0.10}\text{Cr}_{0.01}\text{Fe}^{3+}_{0.09})_{\Sigma 6.00}\text{Si}_6\text{O}_{18}(\text{BO}_3)_3^V(\text{OH})_3^W[\text{O}_{0.50}(\text{OH})_{0.35}\text{F}_{0.15}]_{\Sigma 1.00}$. This ordered formula, used for classification purposes, indicates that the studied sample belongs to the alkali group, alkali-subgroup 1, since $Y = R^{2+}$ and $Z = R^{3+}$. The ratio between monovalent and divalent W-anions is 0.5, thus indicating that it is intermediate between a hydroxy- [(OH) > F] and an oxy-species. The prefix oxy- was preferred in naming it since the ^WO content is very close to be more than 0.5 apfu. Consequently, the studied sample can be classified as (Ni,Fe³⁺)-rich oxy-dravite. Among transition elements, in addition to Fe²⁺, Mn²⁺, V³⁺, Cr³⁺, and Ti⁴⁺, minor Zn²⁺ has also been observed.

The crystal-chemical formula was optimized using the method of Bosi et al. (2017): $^X(\text{Na}_{0.92}\text{Ca}_{0.07}\square_{0.01})_{\Sigma 1.00}^Y(\text{Mg}_{1.21}\text{Al}_{0.80}\text{Ni}_{0.47}\text{Fe}^{3+}_{0.26}\text{Ti}_{0.05}\text{Mn}^{2+}_{0.05}\text{Zn}_{0.05}\text{V}_{0.10}\text{Cr}_{0.01})_{\Sigma 3.00}^Z(\text{Al}_{5.00}\text{Mg}_{0.80}\text{Fe}^{3+}_{0.16}\text{Fe}^{2+}_{0.05})_{\Sigma 6.00}\text{Si}_6\text{O}_{18}(\text{BO}_3)_3^O(\text{OH})_3^{O(1)}[\text{O}_{0.50}(\text{OH})_{0.35}\text{F}_{0.15}]_{\Sigma 1.00}$. The optimized cation site populations are also shown in Tab. 3, where their reliability is supported by mean atomic numbers and mean bond lengths, and weighted bond-valence sums reported in Tab. 4. It is worth noting that the ^W(OH) content calculated from the empirical equation of Bosi (2013), i.e.,

Tab. 3 Optimized cation site populations (atoms per formula unit), mean atomic numbers, and mean bond-lengths (in Å) for (Ni,Fe³⁺)-rich oxy-dravite

Site	Site population	Mean atomic number		Mean bond length	
		Obs.	Calc.	Obs.	Calc.
<i>X</i>	0.92 Na + 0.07 Ca + 0.01 □	11.54(22)	11.53		
<i>Y</i>	1.21 Mg + 0.47 Ni ²⁺ + 0.05 Mn ²⁺ + 0.05 Zn + 0.80 Al + 0.26 Fe ³⁺ + 0.10 V ³⁺ + 0.01 Cr ³⁺ + 0.05 Ti ⁴⁺	17.01(10)	17.06	2.021	2.024 ^a
<i>Z</i>	5.00 Al + 0.16 Fe ³⁺ + 0.80 Mg + 0.05 Fe ²⁺	13.25(8)	13.31	1.930	1.932 ^a
<i>T</i>	6.00 Si	14 ^b	14.00		
<i>B</i>	3 B	5 ^b	5		

^a Calculated from the empirical ionic radii (in Å) of Bosi (2018): Al = 0.547, Fe³⁺ = 0.675, Fe²⁺ = 0.776, Mn²⁺ = 0.809, Zn = 0.740, V = 0.655, Cr = 0.615, Ti = 0.605; the mean *Y* and *Z* anion radii are functions of constituent-anion radius (1.361 and 1.357 Å, respectively). The ionic radius of Ni²⁺ = 0.69 Å from Shannon (1976).

^b Fixed in the final stages of refinement.
Obs. = observed; Calc. = calculated

Tab. 4 Weighted bond-valences (valence units, *vu*) for (Ni,Fe³⁺)-rich oxy-dravite.

Site	<i>X</i>	<i>Y</i>	<i>Z</i>	<i>T</i>	<i>B</i>	Sum
O(1)		0.438 ^{*3} →				1.314
O(2)	0.160 ^{*3} ↓	0.414 ^{*2} ↓→			1.029	2.017
O(3)		0.311	0.407 ^{*2} →			1.125
O(4)	0.071 ^{*3} ↓			0.999 ^{*2} →		2.068
O(5)	0.087 ^{*3} ↓			0.957 ^{*2} →		2.002
O(6)		0.422 ^{*2} ↓	0.517	1.053		1.992
O(7)			0.506	1.056		2.000
O(8)			0.438			
			0.480			
			0.515		0.986 ^{*2} ↓	1.981
Sum	0.952	2.421	2.862	4.066	3.001	
MAV ^a	1.060	2.426	2.859	4.000	3.000	

Note: weighted bond valence according to Bosi (2014). Bond-valences obtained from the bond-valence parameters of Gagné and Hawthorne (2015) for cations bonded to O²⁻ and from Brown and Altermatt (1985) for cations bonded to F⁻. MAV = Mean atomic valence.

^a Expected mean atomic valence (or formal charge) from the empirical crystal-chemical formula.

$^w(\text{OH}) = 2 - \{1.01 \times \text{BVS}[\text{O}(1)]\} - 0.21 - \text{F} = 0.31 \text{ apfu}$, agrees with that calculated from the empirical formula (i.e., 0.35 *apfu*) and FTIR results.

Infrared spectroscopy is in accord with the occurrence of (OH) groups at the O(1) site (\equiv W letter). It is known that the strength of the H-bond is related to a frequency shift in the principal (OH)-stretching vibration (e.g., Libowitzky 1999). In the tourmaline crystal structure, the ^{O(1)}(OH) group forms a very weak H-bond (bond strength < 0.05 valence units, *vu*) with O(4) and O(5), whereas the ^{O(3)}(OH) group forms a weak H-bond (bond strength ~ 0.11 *vu*) with the closest O(5) atom (e.g., Gatta et al. 2014). The different strengths of the H-bonds cause a frequency shift of the principal O–H stretching vibration (e.g., Libowitzky 1999). Therefore, the relatively weak vibrational bands above 3600–3650 cm⁻¹ may be assigned to the O(1) site, whereas the strong bands below 3600–3650 cm⁻¹ may be assigned to the O(3) site (e.g., Gonzalez-Carreño et al. 1988; Bosi et al. 2015b). Based on previous studies (e.g., Skogby et al. 2012; Bosi et al. 2016; Watenphul et al. 2016) as well as on the observed site populations (Tab. 3), the FTIR bands of the studied tourmaline may be likely related to the following atomic arrangements:

- i) ~ 3505 cm⁻¹ is assigned to [(^YMg^ZAl^ZAl)-(^YAl^ZAl^ZAl)-(^YAl^ZAl^ZAl)]-^{O(3)}(OH)₃;
- ii) ~ 3561 cm⁻¹ to [(^YMg^ZAl^ZAl)-(^YMg^ZAl^ZAl)-(^YMg^ZAl^ZAl)]-^{O(3)}(OH)₃;
- iii) ~ 3731 cm⁻¹ to ^Y(MgMgAl)-^{O(1)}(OH)-^X(Na);
- iv) ~ 3761 cm⁻¹ to ^Y(MgMgNi)-^{O(1)}(OH)-^X(Na).

4.2. Nickel in tourmaline supergroup minerals

As briefly reported in the Introduction, nickel-bearing tourmaline supergroup minerals are relatively rare. They

are usually related to meta-ultramafic rocks, where they are usually also enriched in Cr (e.g., Jan et al. 1972; Challis et al. 1995; Michailidis et al. 1995). Henry and Dutrow (2001) described dravite from a metamorphosed karstic bauxite occurring on Samos Island (Greece), having 3.53 wt. % NiO, corresponding to 0.47 Ni *apfu*. Baksheev and Kudryatseva (2004) reported up to 3.96 wt. % NiO (= 0.53 Ni *apfu*) from quartz-carbonate veins hosted in propylitized ultramafic rocks in the Berzovskoe Au deposit, Middle Urals, Russia. Oxy-dravite from

the Artana Mn deposit has a Ni content similar to that reported by Henry and Dutrow (2001) and slightly lower than that of the Russian material.

A later structural investigation of the material from the Middle Urals finding, characterized by a lower amount of Ni (NiO = 1.10 wt. %, corresponding to 0.15 *apfu*), was performed by Hughes et al. (2011). It revealed a lowering of symmetry from trigonal *R3m* to triclinic *P1* due to non-equivalence at *Y* and *Z* sites. According to these authors, a first hint of the possible desymmetrization was observed during the refinement of the unit-cell parameters, yielding a γ angle of 119.742(3)°. However, in oxy-dravite from the Artana Mn prospect, such a deviation from the ideal cell was not observed: unconstrained unit-cell parameters, refined based on 8173 reflections in the 2 θ range between 6.38 and 62.98°, are $a = 15.9410(11)$, $b = 15.9307(11)$, $c = 7.2048(5)$ Å, $\alpha = 90.019(3)$, $\beta = 90.031(3)$, $\gamma = 119.982(2)$ °. Moreover, the calculated R_{int} value for trigonal symmetry is 0.0216 and for triclinic symmetry is 0.0181, a negligible difference. As a result, no evidence of lower symmetry in the diffraction data is provided, and hence the crystal structure of the present Ni-rich tourmaline is consistent with *R3m* symmetry.

Hughes et al. (2011) suggested that Ni was mainly hosted at one of the three symmetry-independent *Y* sites (0.112 *apfu*), whereas the remaining amount was disordered over three out of the six independent *Z* sites (0.033, 0.010, and 0.003 *apfu*). Studies on synthetic Ni-tourmalines suggested that Ni²⁺ was preferentially hosted at the *Y* site but that its actual distribution was related to its content. Synthetic tourmaline having ca. 5 wt. % NiO (= 0.81 Ni *apfu*) has Ni²⁺ at the *Y* site, whereas for higher contents (ca. 13.5 and 19 wt. % NiO, corresponding to 2.40 and 2.94 Ni *apfu*) Ni²⁺ occupies both the *Y* and *Z* sites (Rozhdestvenskaya et al. 2012; Vereshchagin et al. 2015). The Italian sample studied

in this work has a NiO content of 3.46 wt. %, with Ni ordered at the Y site (Tab. 3), in line with previous results on synthetic tourmalines and theoretical studies (e.g., Hughes et al. 2011; Rozhdestvenskaya et al. 2012; Vereshchagin et al. 2015; Bačík and Fridichová 2021).

4.3. Genesis of (Ni,Fe³⁺)-rich oxy-dravite

The high Ni content measured in oxy-dravite from the Artana Mn prospect was unsuspected since previous findings of Ni-bearing tourmaline supergroup minerals were reported from metamorphosed ultramafic rocks or from metabauxites (e.g., Henry and Dutrow 2001; Baksheev and Kudryatseva 2004). Such rocks do not occur in the Artana area, where the Marble formation crops out, along with pelagic cherty metalimestone. The Marble formation is formed by platform metalimestone; at its top, karstic dykes and sills were reported by some authors (e.g., Boccaletti et al. 1981; Fazzuoli and Sguazzoni 1981; Molli and Meccheri 2012). In particular, Molli and Meccheri (2012) pointed out the occurrence of Jurassic structures likely representing the expression of a fault zone related to the rifting stage and the drowning of the Early Jurassic carbonate platform, in some cases associated with structures interpreted as due to syn-sedimentary fault activity. In similar environments, Fe–Mn crusts have been described. For instance, Sulli and Interbartolo (2016) reported Fe–Mn concentrations at the top of the carbonate platform in central Western Sicily (Italy), before the onset of pelagic sediments. According to them, the occurrence of Mn may be related to submarine fault-controlled hydrothermal vents.

Iron-manganese crusts are usually enriched in several transition elements, like Ni (e.g., Jenkins 1970; Usui 1979). Unfortunately, no geochemical data are currently available for the Artana Mn ore minerals. However, two other Mn mineralizations occurring in the Apuan Alps show a Ni-enrichment. The first one, studied by Franceschelli et al. (1996) and located in the Monte Corchia area, is hosted in a lower stratigraphic level (i.e., the Norian Breccia di Seravezza Formation) than that where the Artana Mn mineralization occurs. Several transition elements are enriched in the Mn-rich rocks, the most abundant ones being represented by Cu (up to 2967 µg/g) and Ni (up to 744 µg/g). Another Mn-rich outcrop, whose stratigraphic position has not been clearly constrained, is located in the upper part of the Monte Arsiccio mine, where some lenses of Mn-oxides are embedded in metadolostone; in this occurrence, gersdorffite, NiAsS, and its oxidation product annabergite, Ni₃(AsO₄)₂·8H₂O, have been identified, thus supporting a Ni-rich environment.

Likely, Ni measured in oxy-dravite from the Artana Mn prospect was sourced by the Alpine recrystallization of the Mn ores occurring at the top of the Marble For-

mation under greenschist facies metamorphism. Further studies devoted to a better understanding of the actual setting of these small orebodies and their mineralogy and geochemistry, could best address this hypothesis.

5. Conclusions

Nickel- and Fe³⁺-rich oxy-dravite from the Artana Mn prospect (Apuan Alps) is the fourth well-characterized non-pegmatitic tourmaline supergroup minerals from Tuscany. Along with the recently approved new minerals dutrowite (Biagioni et al. 2020), uvite (Bosi et al. 2022b), and magnesio-lucchesiite (Scribner et al. 2021), it suggests that further crystal-chemical investigations on the many tourmaline occurrences from this Italian sector may be able to improve the tourmaline systematics and our understanding of its crystal chemistry. Moreover, the studied sample is one of the Ni-richest so far described and it occurs in a different geological setting concerning the previously-known occurrences for Ni-bearing tourmalines. On one side, this finding clearly indicates that a careful geochemical study may be desirable for a better knowledge of the geological evolution of the small Mn ore deposit located at the top of the Marble Formation, providing new insights into the geological evolution of the northern Apennines; on the other side it testifies, once again, the capability of these cyclosilicates rich in B to record the geochemistry of the crystallizing environments, in agreement with previous studies (e.g., Dutrow and Henry 2011).

Acknowledgments: A. Criscuolo is acknowledged for field assistance. Funding by Sapienza University of Rome (Prog. Università 2020 to F.B.) is gratefully acknowledged. C.B. and F.B. acknowledge funding by the Ministero dell'Istruzione, dell'Università e della Ricerca through the project PRIN 2020 “HYDROX – HYDRous-oxo-components in minerals: adding new pieces to the Earth's H₂O cycle puzzle”, prot. 2020WYL4NY. The editorial handling of Jan Čempírek and the comments of Peter Bačík and Aaron J. Lussier improved the original manuscript.

Electronic supplementary material. Crystallographic information file (CIF) is available online at the Journal web site (<http://dx.doi.org/10.3190/jgeosci.346>).

References

- BAČÍK P, FRIDICHOVÁ J (2021) Cation partitioning among crystallographic sites based on bond-length constraints in tourmaline-supergroup minerals. *Amer Miner* 106: 851–861

- BAKSHEEV IA, KUDRYAVTSEVA OE (2004) Nickeloan tourmaline from the Berezovskoe gold deposit, Middle Urals, Russia. *Canad Mineral* 42: 1065–1078
- BENVENUTI M, LATTANZI P, TANELLI G (1989) Tourmalinite-associated Pb-Zn-Ag mineralization at Bottino, Apuane Alps, Italy: geologic setting, mineral textures, and sulfide chemistry. *Econ Geol* 84: 1277–1292
- BENVENUTI M, COSTAGLIOLA P, LATTANZI P, TANELLI G (1991) Mineral chemistry of tourmalines from the Bottino mining district, Apuane Alps (Italy). *Eur J Mineral* 3: 537–548
- BIAGIONI C, ORLANDI P, CAMARDA S, CHINELLATO M, APPIANI R, DEL CHIARO L, SANGUINETI G (2019) Minerals from marbles of Carrara and the Apuan Alps. *LoGisma Editore, Firenze*, pp 1–144
- BIAGIONI C, BOSI F, MAURO D, SKOGBY H, DINI A, ZACCARINI F (2020) Dutrowite, IMA 2019-082. *CNMNC Newsletter* 53. *Eur J Mineral* 32: 209–213
- BOCCALETTI M, GOSSO G, MORATTI G (1981) Indizi di paleocarsismo nel Marmo delle Alpi Apuane Settentrionali. *Rend Soc Geol Ital* 4: 315–316
- BONAZZI P, GARBARINO C, MENCHETTI S (1992) Crystal chemistry of piemontites: REE-bearing piemontite from Monte Brugiana, Alpi Apuane, Italy. *Eur J Mineral* 4: 23–33
- BOSI F (2013) Bond-valence constraints around the O1 site of tourmaline. *Mineral Mag* 77: 343–351
- BOSI F (2014) Bond valence at mixed occupancy sites. I. Regular polyhedra. *Acta Crystallogr B* 70: 864–870
- BOSI F (2018) Tourmaline crystal chemistry. *Amer Miner* 103: 298–306
- BOSI F, LUCCHESI S (2007) Crystal chemical relationships in the tourmaline group: structural constraints on chemical variability. *Amer Miner* 92: 1054–1063
- BOSI F, SKOGBY H, AGROSI G, SCANDALE E (2012) Tsilaisite, $\text{NaMn}_3\text{Al}_6(\text{Si}_6\text{O}_{18})(\text{BO}_3)_3(\text{OH})_3\text{OH}$, a new mineral species of the tourmaline supergroup from Grotta d’Oggi, San Pietro in Campo, island of Elba, Italy. *Amer Miner* 97: 989–994
- BOSI F, REZNITSKII L, SKLYAROV EV (2013) Oxy-vanadium-dravite, $\text{NaV}_3(\text{V}_4\text{Mg}_2)(\text{Si}_6\text{O}_{18})(\text{BO}_3)_3(\text{OH})_3\text{O}$ crystal structure and redefinition of the ‘vanadium-dravite’ tourmaline. *Amer Miner* 98: 501–505
- BOSI F, SKOGBY H, REZNITSKII L, HÅLENIUS U (2014) Vanadio-oxy-dravite, $\text{NaV}_3(\text{Al}_4\text{Mg}_2)(\text{Si}_6\text{O}_{18})(\text{BO}_3)_3(\text{OH})_3\text{O}$, a new mineral species of the tourmaline supergroup. *Amer Miner* 99, 218–224.
- BOSI F, ANDREOZZI G, AGROSI G, SCANDALE E (2015a) Fluor-tsilaisite, $\text{NaMn}_3\text{Al}_6(\text{Si}_6\text{O}_{18})(\text{BO}_3)_3(\text{OH})_3\text{F}$, a new tourmaline from San Pietro in Campo (Elba, Italy) and new data on tsilaisitic tourmaline from the holotype specimen locality. *Mineral Mag* 79: 89–101
- BOSI F, SKOGBY H, LAZOR P, REZNITSKII L (2015b) Atomic arrangements around the O3 site in Al- and Cr-rich oxy-tourmalines: a combined EMP, SREF, FTIR and Raman study. *Phys Chem Miner* 42: 441–453
- BOSI F, SKOGBY H, BALIĆ-ŽUNIĆ T (2016) Thermal stability of extended clusters in dravite: a combined EMP, SREF and FTIR study. *Phys Chem Miner* 43: 395–407
- BOSI F, REZNITSKII L, HÅLENIUS U, SKOGBY H (2017) Crystal chemistry of Al-V-Cr oxy-tourmalines from Sludyanka complex, Lake Baikal, Russia. *Eur J Mineral* 29: 457–472
- BOSI F, PEZZOTTA F, ALTIERI A, ANDREOZZI GB, BALIRANO P, TEMPESTA G, CEMPÍREK J, ŠKODA R, FILIP J, ČOPJAKOVÁ R, NOVÁK M, KAMPF AR, SCRIBNER ED, GROAT LA, EVANS RJ (2022a) Celleriite, $\square(\text{Mn}^{2+}_2\text{Al})\text{Al}_6(\text{Si}_6\text{O}_{18})(\text{BO}_3)_3(\text{OH})_3(\text{OH})$, a new mineral species of the tourmaline supergroup. *Amer Miner* 107: 31–42
- BOSI F, BIAGIONI C, PEZZOTTA F, SKOGBY H, HÅLENIUS U, CEMPÍREK J, HAWTHORNE FC, LUSSIER AJ, ABDU YA, DAY MC, FAYEK M, CLARK CM, GRICE JD, HENRY DJ (2022b) Uvite, $\text{CaMg}_3(\text{Al}_5\text{Mg})(\text{Si}_6\text{O}_{18})(\text{BO}_3)_3(\text{OH})_3(\text{OH})$, a new, but long-anticipated mineral species of the tourmaline supergroup from San Piero in Campo (Elba Island, Italy). *Mineral Mag*: doi:10.1180/mgm.2022.54
- BROWN ID, ALTERMATT D (1985) Bond-valence parameters obtained from a systematic analysis of the Inorganic Crystal Structure Database. *Acta Crystallogr B* 41: 244–247
- BRUKER AXS INC. (2016) APEX 3. Bruker Advanced X-ray Solutions, Madison, Wisconsin, USA.
- CARMIGNANI L, KLIGFIELD R (1990) Crustal extension in the northern Apennines: the transition from compression to extension in the Alpi Apuane core complex. *Tectonics* 9: 1275–1303
- CHALLIS A, GRAPES R, PALMER K (1995) Chromian muscovite, uvarovite, and zincian chromite: products of regional metasomatism in Northwest Nelson, New Zealand. *Canad Mineral* 33: 1263–1284
- CONTI P, CARMIGNANI L, MASSA G, MECCHERI M, PATACCA E, SCANDONE P, PIERUCCIONI D (2019) Note illustrative della Carta Geologica d’Italia alla scala 1:50.000. Foglio 249 Massa Carrara. Servizio Geologico d’Italia, Roma, pp 1–290
- D’ACHIARDI G. (1894) Le tormaline del granito elbano. *Atti Soc Tosc Sci Nat Mem* 13: 229–321
- D’ACHIARDI G (1897) Le tormaline del granito elbano. Parte II. *Atti Soc Tosc Sci Nat Mem* 15: 3–74
- DI GIOVANNI F (1981) I minerali del Monte Brugiana. *Riv Mineral Ital* 5: 67–70
- DUTROW BL, HENRY DJ (2011) Tourmaline: A geologic DVD. *Elements* 7: 301–306
- FAZZUOLI M, SGUAZZONI G (1981) Presenza di facies tipo “Rosso Ammonitico” e di forme paleocarsiche al tetto dei marmi in località Pianellaccio (M. Pisanino – Alpi Apuane). *Boll Soc Geol It* 100: 556–566
- FELLIN MG, REINERS PW, BRANDON MT, WÜTHRICH E,

- BALESTRIERI ML, MOLLI G (2007) Thermochronologic evidence for exhumational history of the Alpi Apuane metamorphic core complex, northern Apennines, Italy. *Tectonics* 26: TC6015.
- FRANCESCHELLI M, PUXEDDU M, CARCANGIU G, GATTIGLIO M, PANNUTI F (1996) Breccia-hosted manganese-rich minerals of Alpi Apuane, Italy: A marine, redox-generated deposit. *Lithos* 37: 309–333
- FRANCESCHELLI M, GIANELLI G, PANDELI E, PUXEDDU M (2004) Variscan and Alpine metamorphic events in the northern Apennines (Italy): a review. *Period Mineral* 73: 43–56
- GAGNÉ OC, HAWTHORNE FC (2015) Comprehensive derivation of bond-valence parameters for ion pairs involving oxygen. *Acta Crystallogr B* 71: 562–578
- GATTA GD, BOSI F, MCINTYRE GJ, SKOGBY H (2014) First accurate location of two proton sites in tourmaline: A single-crystal neutron diffraction study of oxy-dravite. *Mineral Mag* 78: 681–692
- GONZALEZ-CARREÑO T, FERNANDEZ M, SANZ J (1988) Infrared and electron microprobe analysis in tourmalines. *Phys Chem Miner* 15, 452–460
- HENRY DJ, DUTROW BL (2001) Compositional zoning and element partitioning in nickeloan tourmaline from a metamorphosed karstbauxite from Samos, Greece. *Amer Miner* 86: 1130–1142
- HENRY DJ, NOVÁK M, HAWTHORNE FC, ERTL A, DUTROW BL, UHER P, PEZZOTTA F (2011) Nomenclature of the tourmaline-super-group minerals. *Amer Miner* 96: 895–913
- HUGHES JM, RAKOVAN J, ERTL A, ROSSMAN GR, BAKSHEEV I, BERNHARDT H-J (2011) Dissymmetrization in tourmaline: the atomic arrangement of sectorally-zoned triclinic Ni-bearing dravite. *Canad Mineral* 49: 29–40
- JAN QM, KEMP DRC, SYMES RF (1972) A chromian tourmaline from Swat, W. Pakistan. *Mineral Mag* 38: 756–759
- JENKINS HC (1970) Fossil manganese nodules from the West Sicilian Jurassic. *Ecl geol Helv* 63: 741–774
- KLIGFIELD R, HUNZIKER J, DALLMEYER R, SCHAMEL S (1986) Dating of deformation phases using the K/Ar and ⁴⁰Ar/³⁹Ar techniques: Results from northern Apennines. *J Struct Geol* 8: 781–798
- LIBOWITZKY E (1999) Correlation of O–H stretching frequencies and O–H···O hydrogen bond lengths in minerals. *Monat Chem* 130: 1047–1059
- MATTSON SM, ROSSMAN GR (1984) Ferric iron in tourmaline. *Phys Chem Miner* 11: 225–234
- MATTSON SM, ROSSMAN GR (1987) Fe²⁺–Fe³⁺ interactions in tourmaline. *Phys Chem Miner* 14: 163–171
- MICHAILIDIS K, SLAVOUNOS S, PLIMER I (1995) Chromian dravite from the chromite ores of Vavdos area, Chalkidiki peninsula, northern Greece. *Neu Jb Mineral, Mh* 1995: 513–528
- MOLLI G, MECCHERI M (2012) Structural inheritance and style of reactivation at mid-crustal levels: A case study from the Alpi Apuane (Tuscany, Italy) *Tectonophysics* 579: 74–87
- ORLANDI P (1990) Zibaldone di mineralogia italiana. *Riv Mineral Ital* 13: 137–144
- ORLANDI P, DINI A (2004) Die Mineralien der Buca della Vena-Mine, Apuaner Berge, Toskana (Italien). *Lapis* 29: 11–24
- PESQUERA A, GIL-CRESPO PP, TORRES-RUIZ F, TORRES-RUIZ J, RODA-ROBLES E (2016) A multiple regression method for estimating Li in tourmaline from electron microprobe analyses. *Mineral Mag* 80: 1129–1133
- POUCHOU JL, PICOIR F (1985) “PAP” (jρZ) procedure for improved quantitative microanalysis. In: ARMSTRONG JT (ed) *Microbeam Analysis*. San Francisco Press, San Francisco, pp 104–106
- ROZHDESTVENSKAYA IV, SETKOVA TV, VERESHCHAGIN OS, SHTUKENBERG AG, SHAPOVALOV YUB (2012) Refinement of the crystal structures of synthetic nickel- and cobalt-bearing tourmalines. *Crystallogr Rep* 57: 57–63
- SCRIBNER ED, CEMPÍREK J, GROAT LA, EVANS RJ, BIAGIONI C, BOSI F, DINI A, HÅLENIUS U, ORLANDI P, PASERO M (2021) Magnesio-lucchesiite, CaMg₃Al₆(Si₆O₁₈)(BO₃)₃(OH)₃O, a new species of the tourmaline super-group. *Amer Miner* 106: 862–871
- SHANNON RD (1976) Revised effective ionic radii and systematic studies of interatomic distances in halides and chalcogenides. *Acta Crystallogr A* 32: 751–767
- SHELDRIK GM (2015) Crystal Structure Refinement with SHELXL. *Acta Crystallogr C* 71: 3–8
- SKOGBY H, BOSI F, LAZOR P (2012) Short-range order in tourmaline: a vibrational spectroscopic approach to elbaite. *Phys Chem Miner* 39: 811–816
- SULLI A, INTERBARTOLO F (2016) Subaerial exposure and drowning processes in a carbonate platform during the Mesozoic Tethyan rifting: The case of the Jurassic succession of Western Sicily (central Mediterranean). *Sediment Geol* 331: 63–77
- TARAN MN, LEBEDEV AS, PLATONOV AN (1993) Optical absorption spectroscopy of synthetic tourmalines. *Phys Chem Miner* 20: 209–220
- USUI A (1979) Nickel and copper accumulation as essential elements in 10-Å manganite of deep-sea manganese nodules. *Nature* 279: 411–413
- VERESHCHAGIN OS, FRANK-KAMENETSKAYA OV, ROZHDESTVENSKAYA IV (2015) Crystal structure and stability of Ni-rich synthetic tourmaline. Distribution of divalent transition-metal cations over octahedral positions. *Mineral Mag* 79: 997–1006
- VERNADSKY W (1913) Über die chemische Formel der Turmaline. *Z Kristallogr Mineral* 53: 273–288
- VEZZONI S, BIAGIONI C, D’ORAZIO M, PIERUCCIONI D, GALANTI Y, PETRELLI M, MOLLI G (2018) Evidence of Permian magmatism in the Alpi Apuane metamorphic complex (Northern Apennines, Italy): New hints for the

- geological evolution of the basement of the Adria plate. *Lithos* 318–319: 104–123
- VOUDOURIS P, MAVROGONATOS C, GRAHAM I, GIULIANI G, TARANTOLA A, MELFOS V, KARAMELAS S, KATERINOPOULOS A, MAGGANAS A. (2019) Gemstones of Greece: Geology and Crystallizing Environments. *Minerals* 9: 461
- WATENPHUL A, BURGDORF M, SCHLÜTER J, HORN I, MALCHEREK T, MIHAILOVA B (2016) Exploring the potential of Raman spectroscopy for crystallo-chemical analyses of complex hydrous silicates: II. Tourmalines. *Amer Miner* 101: 970–985
- WILSON AJC (1992) *International Tables for Crystallography, Volume C: Mathematical, physical and chemical tables*. Kluwer Academic Publishers, Dordrecht, NL, pp 1–883